Circ J 2006; **70:** 129 – 140

Mechanisms Underlying Nano-Sized Air-Pollution-Mediated Progression of Atherosclerosis

—— Carbon Black Causes Cytotoxic Injury/Inflammation and Inhibits Cell Growth in Vascular Endothelial Cells ——

Hideyuki Yamawaki, PhD; Naoharu Iwai, MD

Background Epidemiological studies indicate a significant link between exposure to environmental air pollution and mortality and morbidity from ischemic heart disease. Because nanoparticles can translocate into blood circulation, the present study aimed to clarify their direct effects on human vascular endothelial cells (ECs).

Methods and Results Human umbilical vein ECs (HUVECs) were treated with carbon black (CB), a component of diesel exhaust particles, for 24 h. CB induced cytotoxic morphological changes such as cytosolic vacuole formation, cell disorientation and decreased density. Lactate dehydrogenase assay revealed that CB induced cytotoxic injury in both the cells and plasma membranes. Proliferation assay showed that CB inhibited cell growth. Monocyte chemoattractant protein-1 but not vascular cell adhesion molecule-1 was induced by CB. CB reduced the expressions of connexin37 and endothelial nitric oxide (NO) synthase. Microarray analysis revealed the induction of pro-inflammatory molecules by CB.

Conclusions The present results demonstrate for the first time that CB directly affects the endothelium, causing cytotoxic injury, inflammatory responses, and inhibition of cell growth. As EC injury/inflammation and membrane disintegration are related to the initiation of atherosclerosis, and NO is anti-atherogenic and anti-thrombogenic, the direct effects of nanoparticles on ECs may represent one mechanism behind environmental air pollution-mediated atherosclerosis and ischemic heart disease. (*Circ J* 2006; **70:** 129 – 140)

Key Words: Air pollution; Atherosclerosis; Cell death; Endothelium; Inflammation

According to epidemiological studies in the United States and Europe[1,2] modest rises in the mass of particulate matter (PM) are associated with increases in hospitalizations and mortality because of cardiovascular diseases. The absolute number of deaths attributable to PM is much higher for cardiovascular than for respiratory causes[3,4] Traffic-derived nano-sized particles are most likely responsible for the cardiovascular effects because of their larger surface area, potentially leading to the enhanced biological toxicity[5]

Several mechanisms have been proposed; for example, inhaled particles accumulating in the lungs may cause systemic inflammation via oxidative stress, which mediates endothelial dysfunction and atherosclerosis[1,6] The systemic inflammation may also increase blood coagulability by activating platelets and coagulation factors such as fibrinogen[1,6] In addition, some of the cardiovascular effects of PM involve enhancement of autonomic nervous systems via pulmonary reflexes, leading to the arrhythmia[1,7] However, these mechanisms have not been precisely examined.

More recently, Nemmar et al demonstrated that nano-sized particles translocate from the lungs into the blood[1,8,9] and these particles are barely recognized by phagocytosing cells, such as macrophages, compared with micro-sized particles[5] Therefore, because of the low uptake by macrophages, nanoparticles appear to be taken up by epithelial or endothelial cells (ECs) and thus may directly interact with ECs to induce injury and inflammation, promote thrombosis and destabilize atheromatous plaques. However, the effects on vascular ECs have not been precisely examined and so the present study focused particularly on the direct effects of traffic-derived nanoparticles on cultured vascular ECs in order to explore the cellular mechanisms responsible for air pollution-mediated cardiovascular diseases. This study is relevant given that exposure to nano-materials is rapidly increasing, with benefits to medicine from nanotechnology such as imaging and drug delivery[5,10]

(Received July 15, 2005; revised manuscript received September 22, 2005; accepted October 13, 2005)

Department of Epidemiology, Research Institute, National Cardiovascular Center, Suita, Japan

Mailing address: Naoharu Iwai, MD, PhD, Department of Epidemiology, Research Institute, National Cardiovascular Center, Suita 565-8565, Japan. E-mail: iwai@ri.ncvc.go.jp

Methods

Materials

Carbon black (CB; The Association of Powder Process Industry and Engineering, Japan) was suspended in culture medium by sonication and vortexing. CB is a mimetic of soot-like PM derived from the incomplete combustion of diesel engines. Particle size was measured by a Particle Size Analyzer (UPA-EX150, Nikkiso, Japan), revealing a mean diameter ± SD of 248.2±161.4 nm (50% accumulation, Fig 1). Antibody sources were as follows: eNOS, VCAM-1, and total actin (Santa Cruz Biotech, CA, USA); proliferating cell nuclear antigen (PCNA: BD Bioscience, CA, USA); and connexin37 (Alpha Diagnostica, TX, USA).

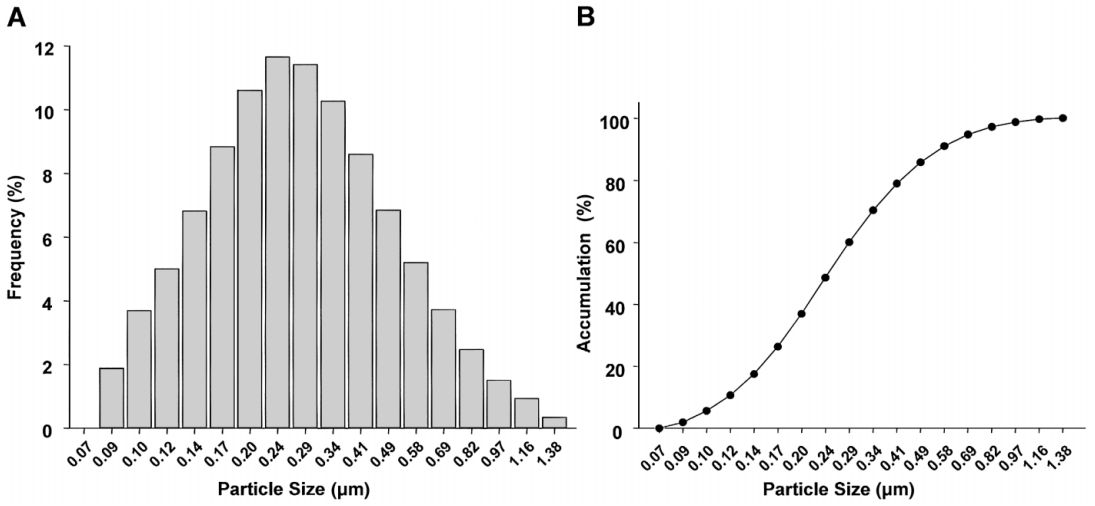

Fig 1. Particle size of carbon black suspended in culture medium. (A) Frequency, (B) accumulation.

Cell Culture

Human umbilical vein ECs (HUVECs) were purchased from Cascade Biologics and cultured in Medium 200 supplemented with low serum growth supplement (LSGS; Cascade Biologics, OR, USA) as described previously.[11] Cells at passages 3–6 were used for experiments.

Electron Microscopy

HUVECs in 60-mm dishes were fixed in 0.1 mol/L sodium cacodylate-buffered (pH7.4) 2.0% glutaraldehyde solution at 4°C overnight and postfixed in 0.1 mol/L sodium cacodylate-buffered (pH7.4) 1% OsO_4 solution at 4°C for 2 h. After dehydration in an ethanol gradient (50–100% each 10 min), samples were embedded in EPON812 at 60°C for 2 days. Ultrathin sections (80 nm) were stained with uranyl acetate and lead citrate. Sections were examined in a JEOL JEM2000EX at 100 kV.

Cytotoxicity Assay

The cytotoxicity assay was performed using a CytoTox 96 non-radioactive cytotoxicity assay kit (Promega, WI, USA) in accordance with the manufacturer's instructions. Briefly, after treating HUVECs at approximately 90% confluence in 6-well plates with CB (1–100 μg/ml) for 24 h, the culture medium was collected and the level of lactate dehydrogenase (LDH), a stable cytosolic enzyme that is released during cell lysis, was measured at absorbance 490 nm using a standard 96-well plate reader. Maximal LDH release was assessed by freeze–thaw lysis of cells, and cytotoxicity was expressed relative to this maximal LDH release.

Proliferation Assay

The proliferation assay was performed using a Cell Counting-8 Kit (Dojindo Laboratories, Japan) according to the manufacturer's instructions. Briefly, after treating HUVECs at approximately 30% confluence in 12-well plates with CB (1–100 μg/ml) for 24 h, water-soluble tetrazolium salt (WST-8) was added for 3 h and the culture medium was collected. Conversion of tetrazolium salt into formazan by living cells (active mitochondria) was measured using a standard 96-well plate reader at absorbance 450 nm. The total number of living cells was shown relative to an untreated control sample.

Western Blotting

Western blotting was performed as described previously.[12] Proteins were obtained by homogenizing HUVECs with Triton-based lysis buffer (1% Triton X-100, 20 mmol/L Tris, pH7.4, 150 mmol/L NaCl, 1 mmol/L EDTA, 1 mmol/L EGTA, 2.5 mmol/L sodium pyrophosphate, 1 mmol/L β-glycerol phosphate, 1 mmol/L Na_3VO_4, 1 μg/ml leupeptin, and 0.1% protease inhibitor mixture; Nacalai Tesque, Japan). Protein concentration was determined using the bicinchoninic acid method (Pierce, IL, USA). Equal amounts of proteins (15 μg) were separated by SDS-PAGE (7.5%) and transferred to a nitrocellulose membrane (Pall Corporation, MI, USA). After blocking with 5% bovine serum albumin, membranes were incubated with primary antibody (1:1,000 dilution) at 4°C overnight, and membrane-bound antibodies were visualized using horseradish peroxidase-conjugated secondary antibodies (1:10,000 dilution, 1 h) and the ECL system (Amersham Biosciences, UK). The resulting autoradiograms were analyzed using NIH Image 1.63 software. Experiments were performed at least 3 times and equal loading of protein was ensured by measuring total actin expression.

Quantitative Determination of Monocyte Chemoattractant Protein (MCP)-1 Release

The MCP-1 protein level was measured using an ELISA kit (Biosource, CA, USA) in accordance with the manufacturer's instructions. Briefly, after treating HUVECs at approximately 90% confluence in 6-well plates with CB (100 μg/ml) for 24 h, the culture medium was collected and the level of MCP-1 was measured at absorbance 450 nm using a standard 96-well plate reader.

Microarray Analysis

Total RNA was isolated from HUVECs treated with or without CB (100 μg/ml, 24 h) using RNeasy Kit (QUIAGEN Inc, CA, USA) according to the manufacturer's instructions. Only samples with an A260/A280 between 1.7 and 2.2 (measured in 10 mmol/L Tris-HCl, pH7.6) were considered suitable for use. Hybridization samples were prepared according to the GeneChip Expression Analysis Technical Manual, 701021 Rev.5 (Section 2: Eukaryotic Sample and Array Processing, Chapter 1: Eukaryotic Target Preparation; http://www.affymetrix.com/support/technical/manuals.affx).

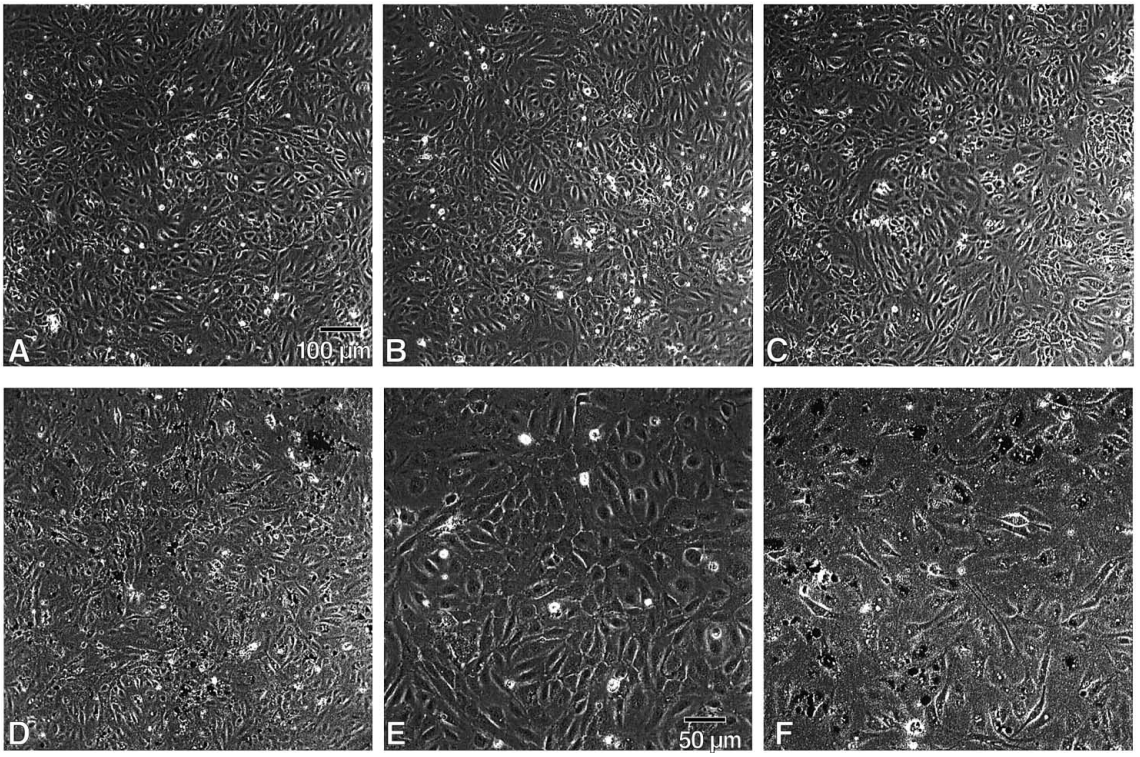

Fig 2. Representative photomicrographs of human umbilical vein endothelial cells (HUVECs) treated with carbon black (CB). HUVECs at ~90% confluence were treated with CB (A,E: 0 μg/ml; B: 1 μg/ml; C: 10 μg/ml; D,F: 100 μg/ml) for 24 h. Scale bar: 100 μm (A–D) and 50 μm (E,F).

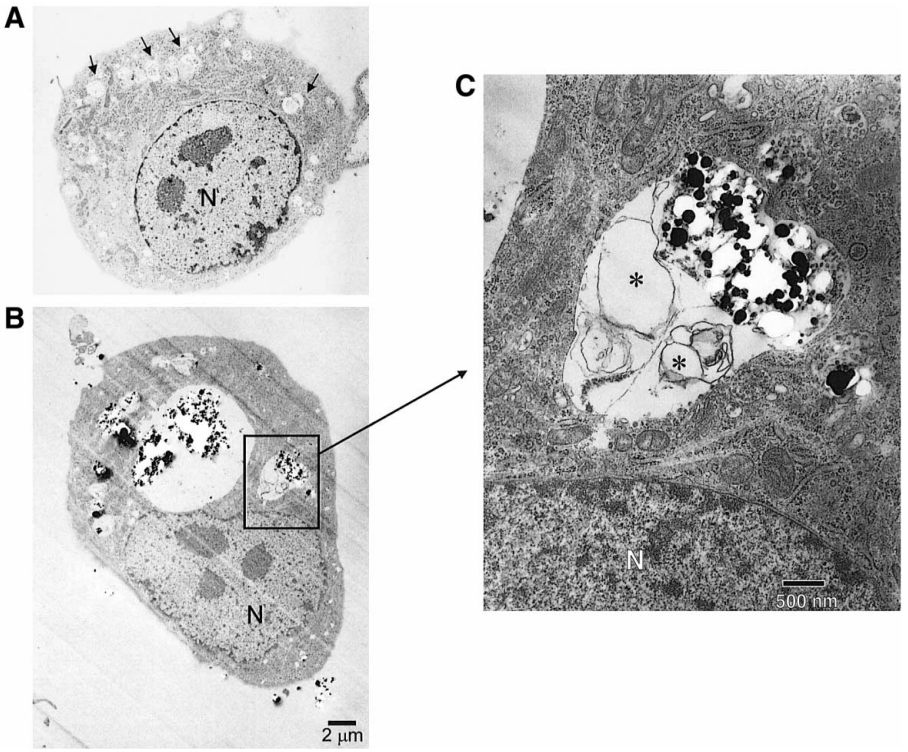

Fig 3. Ultrastructural features of human umbilical vein endothelial cells (HUVECs) treated with carbon black (CB). HUVECs were treated without (A, control) or with 100 μg/ml CB (B, C) for 24 h. Arrows, autophagic vacuoles; (*) membranous whorls. N, nucleus. Scale bar: 2 μm (A,B) and 500 nm (C).

Total RNA (2 μg) was amplified for each sample; cRNA (30 μg) was fragmented in 40 μl of 1× fragmentation buffer. Hybridization cocktails were made as described in the GeneChip Expression Analysis Technical Manual, 701021 Rev.5 (Section 2, Chapter 2: Eukaryotic Target Hybridization) and hybridized to Human genome U133 plus2.0 chips at 60 rpm, 45°C for 16 h using the Hybridization Oven 640 110 V (Affymetrix 800138). The Human genome U133 plus2.0 chips comprise 54,000 probe sets and provide comprehensive coverage of the transcribed human genome on a

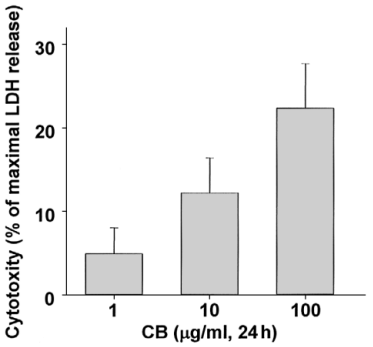

Fig 4. Carbon black (CB) induced cytotoxic injury in human umbilical vein endothelial cells (HUVECs) in a dose-dependent manner. HUVECs at ~90% confluence were treated with CB (1–100 μg/ml) for 24 h. Lactate dehydrogenase (LDH) released into supernatant was measured and maximal LDH release was assessed by freeze–thaw lysis of cells. Cytotoxicity was expressed relative to maximal LDH release (n=6–8).

single array to analyze the expression level of more than 47,000 transcripts and variants, including 38,500 well-characterized human genes plus approximately 6,500 new genes. GeneChips were stained with streptavidin-phycoerythrin using the Fluidics Station 450 (Affymetrix 00-0079). After extensive washing, GeneChips were scanned using a GeneChip Scanner 3000 (Affymetrix 00-0074) and the data were analyzed using the GeneChip Operating Software version 1.1 (Affymetrix 690036) according to the GeneChip Expression Analysis Data Analysis Fundamentals (Chapter 4: First-Order Data Analysis and Data Quality Assessment and Chapter 5: Statistical Algorithms Reference; http://www.affymetrix.com/support/technical/manuals.affx). To allow comparison, all chips were scaled to a target intensity of 500 based on all probe sets on each chip. Comparison of the GeneChip array data was obtained using the KURABO custom analysis services (KURABO Industries Ltd, Osaka, Japan, the authorized service provider of Affymetrix Japan K.K., Tokyo, Japan). Hierarchical cluster analysis was performed using Avadis Software version 3.3 for Windows (proprietary product of Strand Genomics Pvt. Ltd, Bangalore, India). Genes that were significantly upregulated by more than 2-fold (top 89 genes, Table 1, Fig 9A) or downregulated by more than –0.5-fold (top 99 genes, Table 2, Fig 9B) in 2 independent experiments are summarized.

Statistical Analysis

Data are shown as mean ± SEM. Statistical evaluations were performed using unpaired Student's t-test and values of $p<0.05$ were considered statistically significant.

Results

Effects of CB on HUVECs

Cytotoxic Morphological Changes To examine the direct effects of environmental air pollution on vascular ECs, cultured HUVECs were treated with CB (1–100 μg/ml) for 24 h. This induced cytotoxic morphological changes such as cytosolic vacuole formation, cell disorientation, and

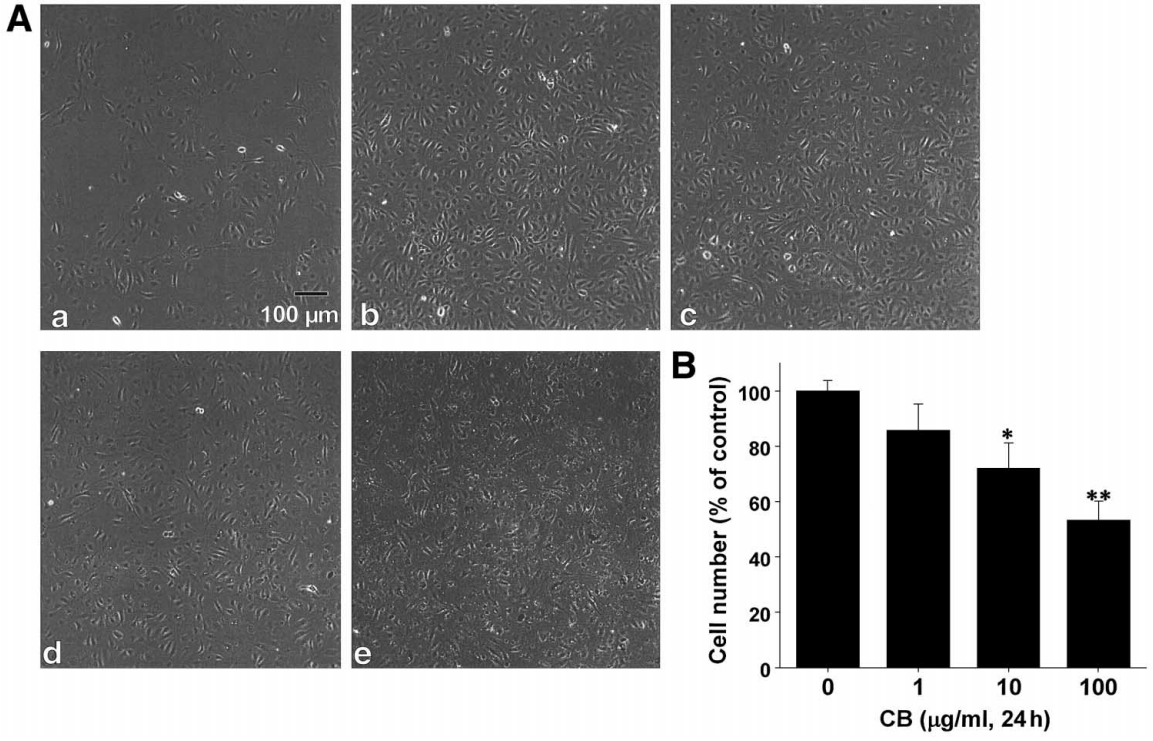

Fig 5. Carbon black (CB) inhibited cell growth in a dose-dependent manner. Human umbilical vein endothelial cells (HUVECs) at ~30% confluence were treated with CB (1–100 μg/ml) for 24 h. (A) Representative photomicrographs of CB for 24 h (a: at start; b: 0 μg/ml; c: 1 μg/ml; d: 10 μg/ml; e: 100 μg/ml). Scale bar: 100 μm (B) Total number of living cells was counted using water-soluble tetrazolium salt (WST-8). Results are shown as percentage relative to control (n=4). *$p<0.05$ and **$p<0.01$ compared with control.

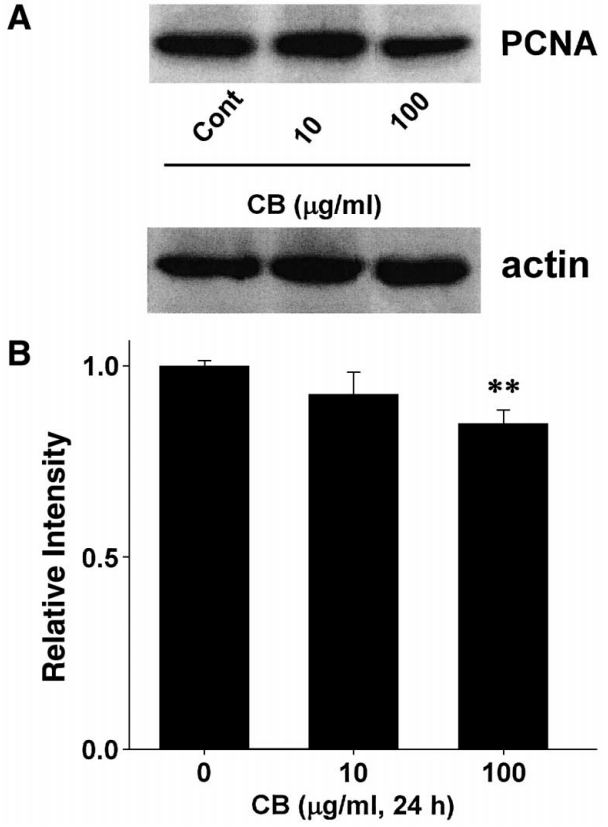

Fig 6. Carbon black (CB) inhibited expression of proliferation marker in human umbilical vein endothelial cells (HUVECs). After HUVECs at ~30% confluence were treated with CB (0, 10 or 100 μg/ml) for 24 h, total cell lysates were harvested. (A) Proliferating cell nuclear antigen (PCNA) expression determined by Western blotting. Equal protein loading was confirmed based on total actin antibody. (B) PCNA expression is shown as the fold-change relative to control (n=7–13). **p<0.01 compared with control.

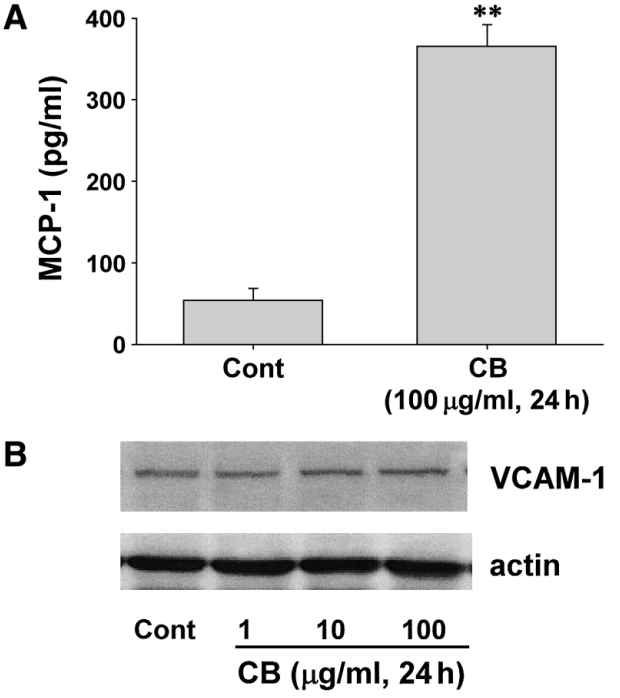

Fig 7. Carbon black (CB) increased proinflammatory chemokine but not leukocyte adhesion molecule in human umbilical vein endothelial cells (HUVECs). After HUVECs at ~90% confluence were treated with CB (1–100 μg/ml) for 24 h, (A) culture medium and (B) total cell lysates were harvested. (A) Monocyte chemoattractant protein (MCP)-1 released into supernatant was measured and its concentration expressed as pg/ml. **p<0.01 compared with control (n=5). (B) Vascular cell adhesion molecule (VCAM)-1 expressions determined by Western blotting. Equal protein loading was confirmed using total actin antibody (n=4).

decreased density in a dose-dependent manner (Fig 2A–F). We next performed an ultrastructural analysis using transmission electron microscopy. The cytoplasm of non-treated HUVECs (control; Fig 3A) contained a number of organelles and small vesicles. It has been reported that in vascular smooth muscle cells the formation of small vesicles occurs under normal physiological conditions for the removal of abnormal proteins and other cytoplasmic macromolecules![13] Treatment of HUVECs with CB (100 μg/ml, 24 h) caused extensive vacuolization and internalization of CB (Fig 3B), mainly within autophagic vacuoles, which contained membranous whorls (Fig 3C). Of note, there were a number of CB particles less than 100 nm within the vacuoles.

Increased Release of LDH To quantitatively assess EC injury by CB, we measured endothelial LDH release, a marker of cell death and injury of the plasma membrane. Treatment of HUVECs with CB (1–100 μg/ml, 24 h) increased LDH release into culture medium in a dose-dependent manner (Fig 4; 5.3±3.1% at 1 μg/ml, 12.2±4.2% at 10 μg/ml, and 22.4±5.3% at 100 μg/ml; n=6–8).

Antiproliferative Effects To examine the effects of CB on cell growth, HUVECs at approximately 30% confluence were treated with CB (1–100 μg/ml) for 24 h and then the total number of living cells was measured using WST-8. HUVECs growth was inhibited in a dose-dependent manner (Fig 5A). Quantitative analysis (Fig 5B) revealed that cell growth was significantly inhibited from 28.0±9.3% (10 μg/ml CB, n=4, p<0.05) to 46.7±7.0% (100 μg/ml CB, n=4, p<0.01). We next examined the effects of CB on the expression of PCNA, which is specifically expressed in the S phase of the cell cycle![14] Western blotting showed that PCNA expression was significantly suppressed by 100 μg/ml CB compared with controls (Fig 6A,B; 15.0±3.5% inhibition, n=13, p<0.01).

Increased Level of Pro-Inflammatory Chemokines We next examined the effects of CB on the expressions of proinflammatory molecules, because in addition to EC injury, inflammation is another key initiating process for atherosclerosis. MCP-1, acting through its receptor CCR2, appears to play an early and important role in the recruitment of monocytes to atherosclerotic lesions![15] and it has been suggested that the serum concentration of MCP-1 is an independent risk factor for progression of atherosclerosis![16] CB (100 μg/ml, 24 h) significantly increased the production of MCP-1 in HUVECs (Fig 7A, 55.1±14.2 pg/ml in control vs 366.0±26.0 pg/ml in CB, n=5, p<0.01). Vascular cell adhesion molecule (VCAM)-1 participate in the recruitment of leukocytes by inducing their firm adhesion to the activated endothelium![17] Western blotting revealed that the expression levels of VCAM-1 were similar between the controls and CB-treated HUVECs (Fig 7B, n=4).

Suppression of Expressions of Gap Junctions and Endothelial NO Synthase (eNOS) Because impairment of the membrane permeability of ECs is crucial for the initiation of atherosclerosis![18,19] the effects of CB on the expression

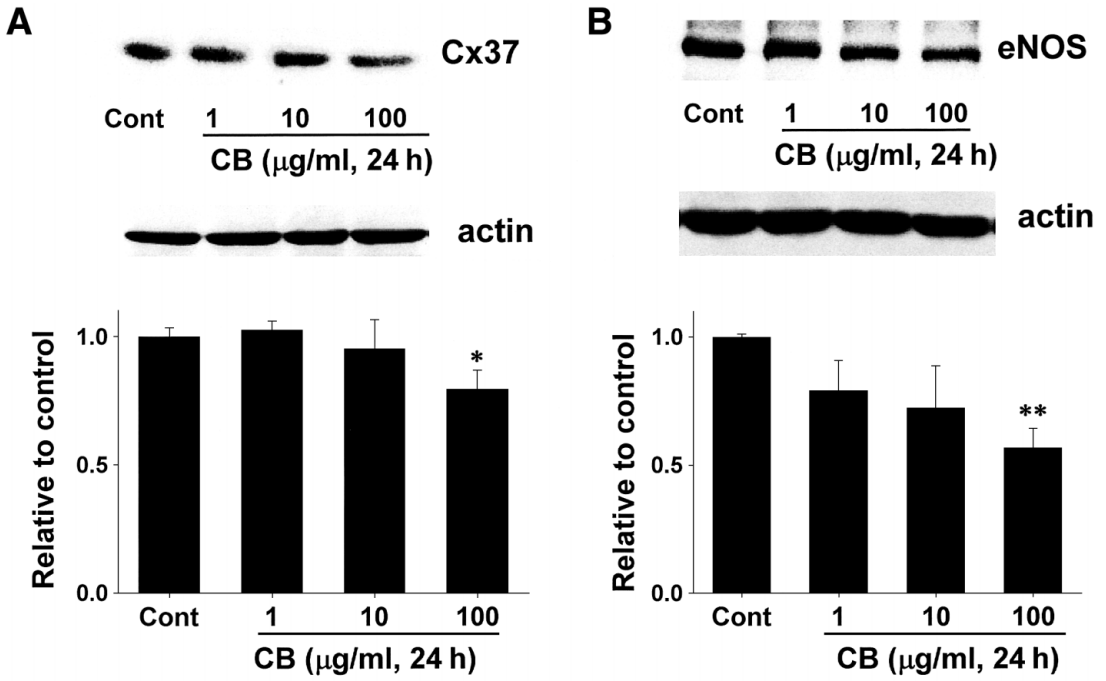

Fig 8. Carbon black (CB) inhibited expressions of connexin37 (Cx37) and endothelial nitric oxide synthase (eNOS) in human umbilical vein endothelial cells (HUVECs). After HUVECs at ~90% confluence were treated with CB (1–100 μg/ml) for 24 h, total cell lysates were harvested. (A) Cx37 and (B) eNOS expressions were determined by Western blotting. Equal protein loading was confirmed using total actin antibody. Expression is shown as the fold-change relative to control (n=4–6 (A) and n=3–5 (B)). *p<0.05 and **p<0.01 compared with control.

Table 1 List of Top 89 Probe Sets Upregulated by Carbon Black (CB) Identified on U133 Chips

Probe set ID	*GenBank accession*	*Gene symbol*	*Gene name*	*Ratio 1 (fold)*	*Ratio 2 (fold)*
200939_s_at	*NM_012102*	*RERE*	*Arginine-glutamic acid dipeptide (RE) repeats*	*2.08*	*3.23*
201566_x_at	*D13891*	*ID2*	*Inhibitor of DNA binding 2, dominant negative helix-loop-helix protein*	*2.25*	*2.39*
202637_s_at	*AI608725*	*ICAM1*	*Intercellular adhesion molecule 1 (CD54), human rhinovirus receptor*	*5.29*	*2.13*
202638_s_at	*NM_000201*	*ICAM1*	*Intercellular adhesion molecule 1 (CD54), human rhinovirus receptor*	*5.20*	*5.33*
202672_s_at	*NM_001674*	*ATF3*	*Activating transcription factor 3*	*3.02*	*4.85*
202768_at	*NM_006732*	*FOSB*	*FBJ murine osteosarcoma viral oncogene homolog B*	*28.41*	*8.97*
202859_x_at	*NM_000584*	*IL8*	*Interleukin 8*	*2.29*	*2.34*
203665_at	*NM_002133*	*HMOX1*	*Heme oxygenase (decycling) 1*	*4.13*	*2.31*
203868_s_at	*NM_001078*	*VCAM1*	*Vascular cell adhesion molecule 1*	*3.96*	*5.39*
204114_at	*NM_007361*	*NID2*	*Nidogen 2 (osteonidogen)*	*2.04*	*2.20*
204472_at	*NM_005261*	*GEM*	*GTP binding protein overexpressed in skeletal muscle*	*4.28*	*4.84*
204595_s_at	*AI300520*	*STC1*	*Stanniocalcin 1*	*2.57*	*2.27*
204622_x_at	*NM_006186*	*NR4A2*	*Nuclear receptor subfamily 4, group A, member 2*	*13.88*	*4.12*
204698_at	*NM_002201*	*ISG20*	*Interferon stimulated gene 20 kDa*	*3.76*	*4.06*
204748_at	*NM_000963*	*PTGS2*	*Prostaglandin-endoperoxide synthase 2 (prostaglandin G/H synthase and cyclooxygenase)*	*3.26*	*2.43*
204802_at	*NM_004165*	*RRAD*	*Ras-related associated with diabetes*	*21.54*	*7.03*
204948_s_at	*NM_013409*	*FST*	*Follistatin*	*3.91*	*3.18*
205290_s_at	*NM_001200*	*BMP2*	*Bone morphogenetic protein 2*	*2.28*	*2.00*
205680_at	*NM_002425*	*MMP10*	*Matrix metalloproteinase 10 (stromelysin 2)*	*2.79*	*2.18*
205822_s_at	*NM_002130*	*HMGCS1*	*3-hydroxy-3-methylglutaryl-Coenzyme A synthase 1 (soluble)*	*3.11*	*2.52*
206211_at	*NM_000450*	*SELE*	*Selectin E (endothelial adhesion molecule 1)*	*9.91*	*4.16*
206463_s_at	*NM_005794*	*DHRS2*	*Dehydrogenase/reductase (SDR family) member 2*	*33.63*	*41.57*
206942_s_at	*NM_002674*	*PMCH*	*Pro-melanin-concentrating hormone*	*7.95*	*5.09*
207148_x_at	*NM_016599*	*MYOZ2*	*Myozenin 2*	*6.87*	*2.54*
207343_at	*NM_020426*	*LYZL6*	*Lysozyme-like 6*	*3.62*	*4.81*
207850_at	*NM_002090*	*CXCL3*	*Chemokine (C-X-C motif) ligand 3*	*3.03*	*2.96*
209189_at	*BC004490*	*FOS*	*V-fos FBJ murine osteosarcoma viral oncogene homolog*	*5.57*	*13.67*
209277_at	*AL574096*	*TFPI2*	*Tissue factor pathway inhibitor 2*	*7.22*	*4.00*
209278_s_at	*L27624*	*TFPI2*	*Tissue factor pathway inhibitor 2*	*5.24*	*3.25*
209419_at	*AB023200*	*C22orf19*	*Chromosome 22 open reading frame 19*	*4.64*	*3.04*
209774_x_at	*M57731*	*CXCL2*	*Chemokine (C-X-C motif) ligand 2*	*2.71*	*2.60*
209785_s_at	*AF065214*	*PLA2G4C*	*Phospholipase A2, group IVC (cytosolic, calcium-independent)*	*2.99*	*2.98*
209795_at	*L07555*	*CD69*	*CD69 antigen (p60, early T-cell activation antigen)*	*2.03*	*2.32*
210139_s_at	*L03203*	*PMP22*	*Peripheral myelin protein 22*	*2.28*	*2.07*

210511_s_at	M13436	INHBA	Inhibin, β A (activin A, activin AB α polypeptide)	2.37	2.81
210675_s_at	U77917	PTPRR	Protein tyrosine phosphatase, receptor type, R	2.18	2.97
211123_at	D87920	SLC5A5	Solute carrier family 5 (sodium iodide symporter), member 5	2.19	2.11
213355_at	AI989567	SIAT10	ST3 β-galactoside α-2,3-sialyltransferase 6	3.45	2.02
213375_s_at	N80918	CG018		2.39	2.13
213782_s_at	BF939176	MYOZ2	Myozenin 2	2.02	3.09
214079_at	AK000345	DHRS2	Dehydrogenase/reductase (SDR family) member 2	20.09	77.60
214321_at	BF440025	NOV	Nephroblastoma overexpressed gene	32.32	5.05
215430_at	AA757089	GK2	Glycerol kinase 2	6.27	12.75
216598_s_at	S69738	CCL2	Chemokine (C-C motif) ligand 2	5.33	4.31
217054_at	AF007194	MUC3B	Mucin 3B	11.59	2.65
217589_at	AW300309	RAB40A	RAB40A, member RAS oncogene family	7.51	3.55
219368_at	NM_021963	NAP1L2	Nucleosome assembly protein 1-like 2	5.99	2.12
219468_s_at	NM_017949	CUEDC1	CUE domain containing 1	2.53	2.11
220014_at	NM_016644	LOC51334		2.31	24.75
220116_at	NM_021614	KCNN2	Potassium intermediate/small conductance calcium-activated channel, subfamily N, member 2	2.75	9.52
220243_at	NM_014155	HSPC063	BTB (POZ) domain containing 15	3.40	3.93
220266_s_at	NM_004235	KLF4	Kruppel-like factor 4 (gut)	2.18	3.64
220542_s_at	NM_016583	PLUNC	Palate, lung and nasal epithelium carcinoma associated	2.18	2.08
221524_s_at	AF272036	RRAGD	Ras-related GTP binding D	4.80	8.50
221555_x_at	AU145941	CDC14B	CDC14 cell division cycle 14 homolog B (S. cerevisiae)	3.04	2.05
221750_at	BG035985	HMGCS1	3-hydroxy-3-methylglutaryl-Coenzyme A synthase 1 (soluble)	2.18	2.15
33304_at	U88964	ISG20	Interferon stimulated gene 20 kDa	2.12	2.01
222486_s_at	AF060152	ADAMTS1	A disintegrin-like and metalloprotease (reprolysin type) with thrombospondin type 1 motif, 1	3.37	2.27
226632_at	AL513673	CYGB	Cytoglobin	2.24	2.05
226731_at	AA156873	PELO	Pelota homolog (Drosophila)	9.41	4.61
226847_at	BF438173	FST	Follistatin	4.32	4.77
226991_at	AA489681	NFATC2	Nuclear factor of activated T-cells, cytoplasmic, calcineurin-dependent 2	3.10	2.04
227140_at	AI343467	INHBA	Inhibin, beta A (activin A, activin AB alpha polypeptide)	2.07	2.17
228038_at	AI669815	SOX2	SRY (sex determining region Y)-box 2	2.23	2.07
230657_at	AI423466	CLOCK	Clock homolog (mouse)	2.29	11.50
230966_at	AI859620	NUP62	Nucleoporin 62kDa	6.24	2.46
231042_s_at	AA809487	CAMK2D	Calcium/calmodulin-dependent protein kinase (CaM kinase) II delta	2.97	2.13
233615_at	AU157698	CGA	Glycoprotein hormones, alpha polypeptide	3.83	4.11
235652_at	AI431345	SCML1	Sex comb on midleg-like 1 (Drosophila)	3.21	22.28
237885_at	AW589793	SOX21	SRY (sex determining region Y)-box 21	10.16	12.97
239998_at	AI990484	C10orf53	Chromosome 10 open reading frame 53	4.23	2.49
240156_at	AA417099	RFX2	Regulatory factor X, 2 (influences HLA class II expression)	5.11	3.05
240793_at	BF224054	TTN	Titin	2.60	4.25
242593_at	AI833186	KIAA0143		5.33	3.38
242792_at	AA004487	NFIB	Nuclear factor I/B	2.60	2.34
244056_at	AW293443	UNQ541		12.21	13.96
244684_at	AI432340	PGGT1B	Protein geranylgeranyltransferase type I, beta subunit	9.05	8.77
1553157_at	AB055703	LHX4	LIM homeobox 4	11.17	4.64
1553428_at	NM_173675	FLJ33708		14.17	14.84
1554514_at	BC013753	FLJ20581		21.23	6.46
1554569_a_at	BC036391	CUGBP2	CUG triplet repeat, RNA binding protein 2	2.18	3.27
1554741_s_at	AF523265	FLJ30435		11.89	2.43
1554804_a_at	BC030524	CLDN19	Claudin 19	2.05	4.42
1554997_a_at	AY151286	PTGS2	Prostaglandin-endoperoxide synthase 2 (prostaglandin G/H synthase and cyclooxygenase)	4.34	2.94
1556773_at	M31157	PTHLH	Parathyroid hormone-like hormone	3.67	2.85
1559121_s_at	AI767566	ARIH2	Ariadne homolog 2 (Drosophila)	2.07	2.36
1561589_a_at	AB053319	NBEAL1	Neurobeachin-like 1	7.70	2.20
1568589_at	AF113014	C10orf74	Chromosome 10 open reading frame 74	7.61	12.19
1570022_at	BC038182	C3orf1	Chromosome 3 open reading frame 1	2.14	23.82

Ratio 1: CB100,24h-1/Control1; Ratio 2: CB100,24h-2/Control2.

of endothelial gap junctions were examined. CB (100 μg/ml, 24 h) significantly inhibited the expression of connexin37 in HUVECs (Fig 8A, 20.8±7.4% inhibition, n=6, $p<0.05$). Endothelium-derived nitric oxide (NO) is known to be anti-atherogenic and anti-thrombogenic;[20] and Western blotting demonstrated that CB (100 μg/ml, 24 h) significantly suppressed eNOS expression (Fig 8B, 43.4±7.7% inhibition, n=5, $p<0.01$).

Microarray Analysis

We performed the microarray analysis using total RNA from HUVECs treated without or with CB (100 μg/ml, 24 h). Results from 2 independent samples are summarized in Tables 1 and 2. Hierarchical cluster analysis of differentially expressed genes is shown in Fig 9A,B. The data showed that several inflammation-related genes, including ICAM1 (intercellular adhesion molecule 1), interleukin 8, HMOX1 (heme oxygenase 1), VCAM-1, PTGS2 (prostaglandin-endoperoxide synthase 2), SELE (selectin E), and CCL2 (chemokine (C-C motif) ligand 2, also known as MCP-1), are significantly upregulated by CB (Table 1). Although changes in the gene expression level for MCP-1 (Table 1), eNOS (NOS3, mean ratio (fold)=0.8, data not shown), and connexin37 (GJA4, mean ratio (fold)=0.8, data

Table 2 List of Top 99 Probe Sets Downregulated by Carbon Black (CB) Identified on U133 Chips

Probe set ID	GenBank accession	Gene symbol	Gene name	Ratio 1 (fold)	Ratio 2 (fold)
203003_at	AL530331	MEF2D	MADS box transcription enhancer factor 2, polypeptide D (myocyte enhancer factor 2D)	0.49	0.42
203876_s_at	AI761713	MMP11	Matrix metalloproteinase 11 (stromelysin 3)	0.19	0.22
204196_x_at	NM_004571	PKNOX1	PBX/knotted 1 homeobox 1	0.45	0.31
205749_at	NM_000499	CYP1A1	Cytochrome P450, family 1, subfamily A, polypeptide 1	0.02	0.35
206679_at	NM_001163	APBA1	Amyloid beta (A4) precursor protein-binding, family A, member 1 (X11)	0.13	0.11
207045_at	NM_017667	FLJ20097		0.37	0.45
207252_at	NM_003669	INE1	Inactivation escape 1	0.33	0.42
207323_s_at	NM_002385	MBP	Myelin basic protein	0.34	0.47
209047_at	AL518391	AQP1	Aquaporin 1 (channel-forming integral protein, 28 kDa)	0.07	0.30
209841_s_at	AL442092	LRRN3	Leucine rich repeat neuronal 3	0.15	0.09
211516_at	M96651	IL5RA	Interleukin 5 receptor, alpha	0.38	0.36
211880_x_at	AF152507	PCDHGC3	Protocadherin gamma subfamily C, 3	0.33	0.13
213517_at	AW103422	PCBP2	Poly(rC) binding protein 2	0.41	0.46
213593_s_at	AW978896	TRA2A		0.38	0.47
213948_x_at	AI564838	IGSF4B	Immunoglobulin superfamily, member 4B	0.48	0.45
214184_at	AW195837	NPFF	Neuropeptide FF-amide peptide precursor	0.30	0.33
215209_at	AU143984	SEC24D	SEC24 related gene family, member D (S. cerevisiae)	0.13	0.48
215567_at	AU144919	C14orf111	Chromosome 14 open reading frame 111	0.20	0.28
215786_at	AK022170	HBXAP	Hepatitis B virus x associated protein	0.39	0.42
216147_at	AL353942	38606	Septin 11	0.20	0.41
219957_at	NM_017987	RUFY2	RUN and FYVE domain containing 2	0.43	0.36
220988_s_at	NM_030945	C1QTNF3	C1q and tumor necrosis factor related protein 3	0.31	0.45
221397_at	NM_023921	TAS2R10	Taste receptor, type 2, member 10	0.40	0.29
226655_at	BF126274	STX17	Syntaxin 17	0.43	0.42
227223_at	BE466173	RNPC2	RNA-binding region (RNP1, RRM) containing 2	0.48	0.46
228030_at	AI041522	RBM6	RNA binding motif protein 6	0.45	0.41
228173_at	AA810695	GNAS	GNAS complex locus	0.28	0.50
229193_at	AA005430	CROP		0.21	0.44
229365_at	BF475372	PPP1R3F	Protein phosphatase 1, regulatory (inhibitor) subunit 3F	0.22	0.35
229894_s_at	AI858067	RAB43	RAB43, member RAS oncogene family	0.32	0.43
229996_s_at	BF196224	PCGF5	Polycomb group ring finger 5	0.40	0.35
230562_at	R45298	MCPH1	Microcephaly, primary autosomal recessive 1	0.31	0.08
230609_at	BF510429	ENTH		0.42	0.24
231400_s_at	BE219311	TIMM22	Translocase of inner mitochondrial membrane 22 homolog (yeast)	0.48	0.42
232059_at	AI433419	DSCAML1	Down syndrome cell adhesion molecule like 1	0.34	0.08
232291_at	AA256157	C13orf25	Chromosome 13 open reading frame 25	0.22	0.36
232757_at	AV705679	MTSS1	Metastasis suppressor 1	0.23	0.35
233193_x_at	AK000455	MGC16733		0.34	0.38
233349_at	AI800481	TLK2	Tousled-like kinase 2	0.09	0.17
233637_at	AU146915	WDR42A	WD repeat domain 42A	0.41	0.37
234047_at	AK024127	SNRP70	Small nuclear ribonucleoprotein 70 kDa polypeptide (RNP antigen)	0.44	0.49
234562_x_at	AK000115	CKLFSF8	Chemokine-like factor super family 8	0.27	0.38
234859_at	AL137352	DKFZp434G0625		0.33	0.40
235926_at	AI312527	ANAPC5	Anaphase promoting complex subunit 5	0.45	0.44
235927_at	BE350122	XPO1	Exportin 1 (CRM1 homolog, yeast)	0.39	0.45
236076_at	AW241549	LOC257396		0.21	0.04
237305_at	AW450381	CDH2	Cadherin 2, type 1, N-cadherin (neuronal)	0.47	0.21
237834_at	BF062366	SNCAIP	Synuclein, α interacting protein (synphilin)	0.43	0.07
238279_x_at	BF062155	COL4A3BP	Collagen, type IV, alpha 3 (Goodpasture antigen) binding protein	0.17	0.46
238513_at	BF905445	PRRG4	Proline rich Gla (G-carboxyglutamic acid) 4 (transmembrane)	0.02	0.05
238563_at	AV762916	TPRT	Trans-prenyltransferase	0.40	0.37
238797_at	BF059582	TRIM11	Tripartite motif-containing 11	0.46	0.34
238982_at	AW665791	DENR	Density-regulated protein	0.08	0.14
239243_at	AA279654	ZNF638	Zinc finger protein 638	0.09	0.12
239441_at	AI359527	LOC284323		0.41	0.33
239448_at	AI475033	SMAD3	SMAD, mothers against DPP homolog 3 (Drosophila)	0.24	0.40
239583_x_at	BG354573	PSG4	Pregnancy specific beta-1-glycoprotein 4	0.49	0.45
239678_at	AL041224	AP1GBP1	AP1 gamma subunit binding protein 1	0.33	0.43
240008_at	AI955765	ARID1B	AT rich interactive domain 1B (SWI1-like)	0.02	0.16
240349_at	AV693202	PRKAA2	Protein kinase, AMP-activated, alpha 2 catalytic subunit	0.49	0.35
240458_at	AI242023	FAM20C	Family with sequence similarity 20, member C	0.49	0.39
240655_at	BE502785	ALCAM	Activated leukocyte cell adhesion molecule	0.08	0.46
241027_at	BE858373	OPA1	Optic atrophy 1 (autosomal dominant)	0.20	0.10
241174_at	AV647279	AP4E1	Adaptor-related protein complex 4, epsilon 1 subunit	0.47	0.07
241757_x_at	AA947051	D2LIC		0.42	0.38
241785_at	AA613520	DNAJC11	DnaJ (Hsp40) homolog, subfamily C, member 11	0.41	0.08
241977_s_at	AI634523	RAB3C	RAB3C, member RAS oncogene family	0.38	0.40
242279_at	R11494	SDFR1	Stromal cell derived factor receptor 1	0.31	0.20
242343_x_at	H57111	ZNF518	Zinc finger protein 518	0.41	0.11
242480_at	AA868356	MYST3	MYST histone acetyltransferase (monocytic leukemia) 3	0.44	0.18

242805_at	*AW081636*	*CCNC*	*Cyclin C*	*0.40*	*0.36*
242937_at	*AV763408*	*FOXK2*	*Forkhead box K2*	*0.34*	*0.43*
243198_at	*AA020920*	*TEX9*		*0.27*	*0.29*
243650_at	*AI217992*	*PLEKHH2*	*Pleckstrin homology domain containing, family H (with MyTH4 domain) member 2*	*0.05*	*0.20*
244778_x_at	*N63691*	*M11S1*	*Membrane component, chromosome 11, surface marker 1*	*0.44*	*0.41*
244803_at	*AI335191*	*YAP*	*YY1 associated protein 1*	*0.48*	*0.41*
1552536_at	*NM_145206*	*VTI1A*	*Vesicle transport through interaction with t-SNAREs homolog 1A (yeast)*	*0.12*	*0.30*
1552621_at	*BQ613856*	*MGC13098*		*0.45*	*0.34*
1552935_at	*NM_152694*	*ZCCHC5*	*Zinc finger, CCHC domain containing 5*	*0.41*	*0.20*
1553145_at	*BC010030*	*FLJ39653*		*0.18*	*0.35*
1553693_s_at	*NM_032783*	*CBR4*		*0.41*	*0.39*
1554328_at	*BC041485*	*STXBP4*	*Syntaxin binding protein 4*	*0.33*	*0.49*
1554707_at	*BC034293*	*C9orf68*	*Chromosome 9 open reading frame 68*	*0.34*	*0.21*
1554960_at	*BC040018*	*MGC48998*		*0.44*	*0.48*
1555878_at	*AK094613*	*RPS24*	*Ribosomal protein S24*	*0.39*	*0.47*
1556088_at	*AK098491*	*RIP*		*0.44*	*0.28*
1556322_a_at	*AW952920*	*TJP4*	*Tight junction protein 4 (peripheral)*	*0.18*	*0.38*
1557223_at	*AK057533*	*RBPMS*	*RNA binding protein with multiple splicing*	*0.38*	*0.33*
1557759_at	*AW102805*	*FLJ10241*		*0.43*	*0.10*
1559063_at	*AL355689*	*C21orf63*	*Chromosome 21 open reading frame 63*	*0.31*	*0.31*
1559691_at	*BC032767*	*NDUFS1*	*NADH dehydrogenase (ubiquinone) Fe-S protein 1, 75 kDa (NADH-coenzyme Q reductase)*	*0.02*	*0.45*
1559746_a_at	*AK096662*	*FLJ90036*		*0.11*	*0.14*
1560776_at	*AU121725*	*HIP2*	*Huntingtin interacting protein 2*	*0.44*	*0.43*
1561175_at	*AK092513*	*LOC283482*		*0.08*	*0.43*
1564272_a_at	*AK098735*	*KLHDC1*	*Kelch domain containing 1*	*0.01*	*0.19*
1564699_at	*BC017920*	*C5orf4*	*Chromosome 5 open reading frame 4*	*0.01*	*0.04*
1568627_at	*BC032531*	*KIAA1387*		*0.47*	*0.44*
1568782_at	*BC027851*	*RP2*	*Retinitis pigmentosa 2 (X-linked recessive)*	*0.39*	*0.15*
1569408_at	*BC016012*	*EIF2C4*	*Eukaryotic translation initiation factor 2C, 4*	*0.07*	*0.10*

Ratio 1: CB100,24h-1/Control1; Ratio 2: CB100,24h-2/Control2.

not shown) were in accordance with those in the protein expression level (Figs 7A,8), that of VCAM-1 (increase, Table 1) was dissociated from the change in protein expression (no difference, Fig 7B). Further validation is necessary by comparing the microarray data with quantitative reverse transcriptase-polymerase chain reaction (RNA level) and/or Western blotting (protein level) data.

Discussion

The major findings of the present study are that CB directly affects vascular ECs, causing cytotoxic injury, inflammatory responses, and inhibition of cell growth. To the best of our knowledge, this is the first demonstration of the direct effects of CB on the vascular endothelium. Novel aspects of this study include the finding that CB increases the production of the inflammatory chemokine, MCP-1, while it suppresses the expressions of gap junctions and eNOS in ECs. Although further validation is necessary, microarray analysis supports the finding that the expression of genes related vascular inflammation is upregulated by CB. Because EC injury, inflammation, and impairment of membrane integrity are closely related to the initiation of atherosclerosis;[18,19] and NO is anti-atherogenic and anti-thrombogenic;[20] the direct effects of nano-sized air pollution on ECs could represent one mechanism by which air pollution exacerbates atherosclerosis and ischemic heart disease (IHD).

We propose that EC injury is most likely mediated via the direct physical contact of CB with the cells, including the internalization of CB and excess autophagic vacuole formation. Because CB has minimal metallic components;[21] it seems unlikely that the effects were mediated by chemical reactions. In addition to the direct effects of CB, it could also be possible that the changes were mediated secondarily via cytokines and/or reactive oxygen species produced by the injured ECs. There is also a report that examined the toxic effects of several nano-materials, including metals (TiO_2, SiO_2, Co, Ni, polyvinyl chloride), on ECs and it showed that only Co particles had a cytotoxic effect on ECs;[22] Thus it seems likely that there are variations in the effects of nano-particles and that our results could be specific to CB.

Associations between EC injury/inflammation and the development of atherosclerosis are well documented.[18,19] Injury and/or denudation of ECs triggers the attachment of leukocytes to the subendothelial region and promotes transendothelial migration of cells (ie, the EC inflammatory process), initiating atherosclerosis. Platelets also readily accumulate where there are injured ECs, which may promote thrombus formation. Interestingly, our results showed that MCP-1 (ie, chemokine for leukocytes) but not VCAM-1 (leukocyte adhesion molecules), was induced by CB, suggesting a specific role of CB in the vascular inflammatory pathways. Impairment of EC growth may be related to impairment of angiogenesis, the formation of new blood vessels, from the existing vascular bed. Because angiogenesis is important for the maintenance of vascular integrity in both wound healing and the formation of collateral vessels in response to tissue ischemia;[23] the present finding that CB inhibits EC growth may indicate an association with the progression of IHD.

In addition to EC injury/inflammation and inhibition of cell growth, we observed that CB suppressed the expression of connexin37 and eNOS protein in the vascular endothelium. Substantial evidence suggests altered expression of gap junctions during atherogenesis. Kwak et al demonstrated in mouse and human atheroma regions that expression of endothelial connexin37 was suppressed compared with normal aorta;[24] Yeh et al[2] also reported reduced expres-

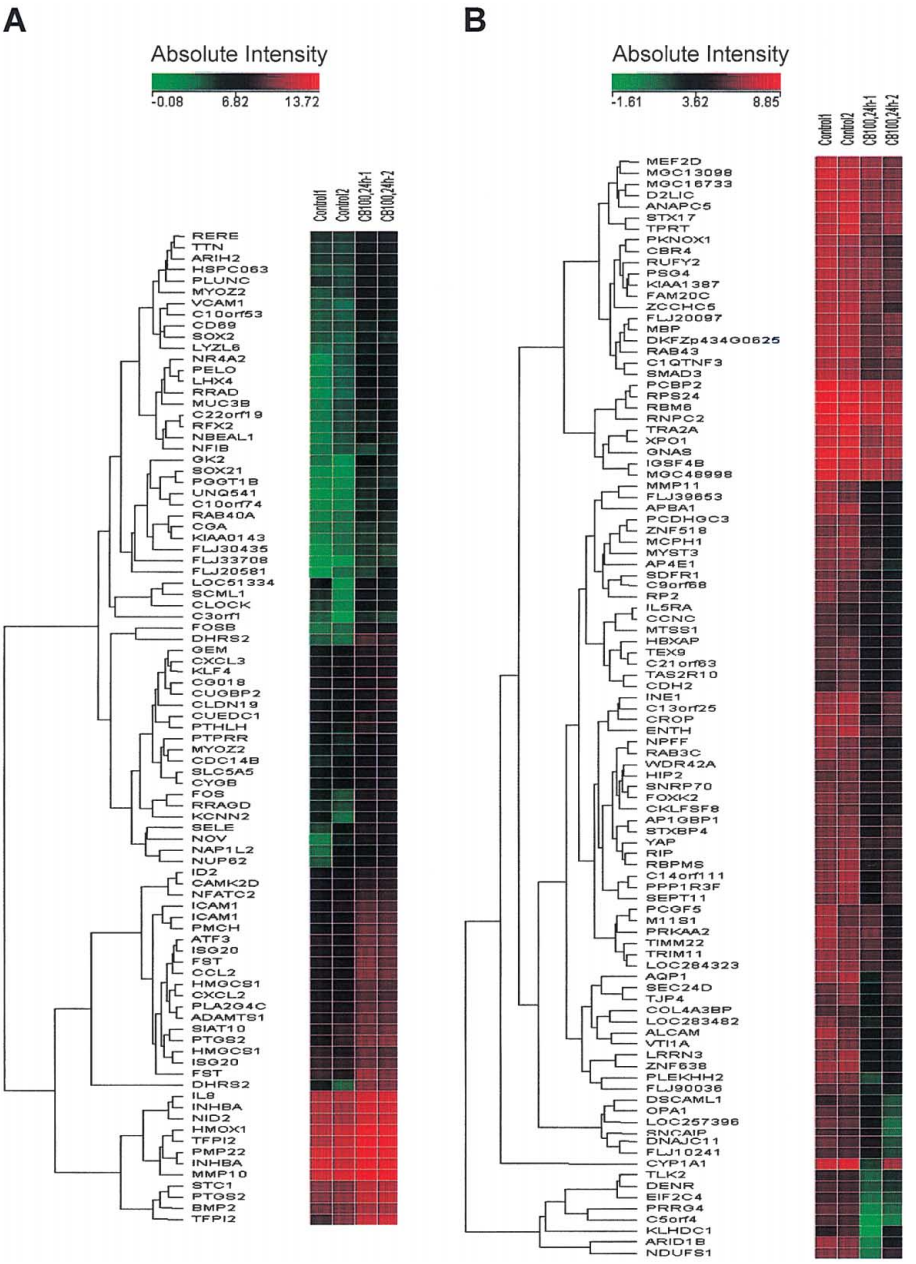

Fig 9. Hierarchical cluster analysis of differentially expressed genes (A) upregulated (top 89 genes) and (B) downregulated (top 99 genes) by carbon black (CB). Total RNA was isolated from human umbilical vein endothelial cells (HUVECs) treated without (Control) or with 100 μg/ml CB (CB100, 24 h) for 24 h. Hierarchical trees were generated using Avadis Software, Version 3.3.

sion of connexin37 in the ECs of hyperlipidemic mouse aorta, and that expression recovered with simvastatin treatment.[25] ECs apparently have to physically uncouple in order to allow transendothelial migration of leukocytes. Inflammatory mediators, such as tumor necrosis factor-α[12,26] and lipopolysaccharide,[27] induce leukocyte adhesion molecules such as VCAM-1, but also downregulate connexin37 expression in vascular ECs.[28,29] The inhibition of connexin37 expression by CB thus seems to be associated with EC inflammatory process such as adhesion and/or transmigration of leukocytes. Finally, a genetic polymorphism has been identified in the human connexin37 protein, apparently representing a prognostic marker for atherosclerotic plaque development.[30]

Impairment of the NO-producing function of ECs is associated with progression of atherosclerosis and IHD via several mechanisms.[31,32] For example, NO is known to inhibit platelet aggregation and thus prevent thrombus formation,[20] and because it inhibits leukocyte adhesion[33] and smooth muscle proliferation,[34] NO is atheroprotective. It has recently been shown that NO regulates large artery stiffness by altering smooth muscle tone.[35] Impairment of the NO-producing function seems likely to increase cardiovascular risk factors by enhancing arterial stiffness, because a number of cardiovascular risk factors, including hypertension[36] and diabetes,[37] are associated with increased stiffness of large arteries. An example of the likely mechanism involves the induction of isolated systolic hypertension, which predominantly results from increased stiffness of large arteries, rather than elevated peripheral vascular resistance. Of note, it has been reported that EC cytotoxicity caused by organic compounds in diesel exhaust particles (DEP), including polyaromatic hydrocarbons, nitroaromatic hydrocarbons, heterocyclics, quinines, aldehydes and aliphatic hydrocarbons, was inhibited by NOS inhibitor, suggesting the involvement of peroxynitrite formation due to the organic

particles-mediated superoxide production[38]

The present study used CB to mimic traffic-derived nanoparticles. Measurement of particle size revealed a mean diameter of approximately 250 nm (50% accumulation, Fig 1). DEP have a similar volume (mass) distribution[39] It was demonstrated by Nemmar et al that particles less than 100 nm in diameter may translocate into the blood circulation[8,9] and recent studies have also demonstrated that such particles are more toxic to cells, presumably because of their larger surface area and greater reactivity.[5] Although the mass distribution of CB <100 nm was only 5.6% in our preparations, the number of smaller sized CB should be much higher than larger sized CB, as shown in DEP[39] The ultrastructural evaluation showed a number of particles <100 nm within the autophagic vacuoles, which supports the concept.

The present study used 1–100 μg/ml of CB for in vitro experiments. Levels of PM ($PM_{2.5}$; particles <2.5 μm) are high, especially in the developing countries such as China. It has been reported that the maximal concentration of $PM_{2.5}$ in Chongqing, one of the biggest cities in China, was 666 $\mu g/ml^3$ (daily average),[40] which indicates that a person can inhale 9,590 μg of $PM_{2.5}$ for 24 h, which is equivalent to 0.8 μg/ml when the extracellular fluid volume is 12 L for a 60 kg person. Thus it is estimated that the CB dosage used in the present study is 1–100-fold higher, but we believe that they are within the pathophysiologic ranges because (1) although the effects of 100 μg/ml CB were very strong, we observed dose-dependent (1–100 μg/ml) effects in the experiments, and (2) CB is hardly metabolized and cumulatively accumulates in EC over time. Inhalation toxicity of CB, especially on the cardiovascular system, needs to be examined.

In summary, the present study examined the direct effects of CB on vascular ECs to determine the mechanisms underlying air pollution-induced increases in atherosclerosis and IHD. We observed CB-mediated cytotoxic, pro-inflammatory, and antiproliferative effects, in addition to inhibition of gap junctions and expression of eNOS proteins, which could represent a possible mechanism. Further examinations using blood vessels and animal models are required to show that traffic-derived nanoparticles have a key role in air-pollution-induced cardiovascular diseases.

Acknowledgments

This study was supported by the Health and Labor Sciences Research Grants: Research on Risk of Chemical Substance (H17-Chemistry-008), Salt Science Research Foundation (05C05), and by a Grant-in-Aid (#17790176) for Scientific Research from the Ministry of Education, Culture, Sports, Science, and Technology, Japan.

References

1. Brook RD, Franklin B, Cascio W, Hong Y, Howard G, Lipsett M, et al. Air pollution and cardiovascular disease: A statement for healthcare professionals from the Expert Panel on Population and Prevention Science of the American Heart Association. *Circulation* 2004; **109:** 2655–2671.
2. Katsouyanni K, Touloumi G, Samoli E, Gryparis A, Le Tertre A, Monopolis Y, et al. Confounding and effect modification in the short-term effects of ambient particles on total mortality: Results from 29 European cities within the APHEA2 project. *Epidemiology* 2001; **12:** 521–531.
3. Dockery DW. Epidemiologic evidence of cardiovascular effects of particulate air pollution. *Environ Health Perspect* 2001; **109**(Suppl 4)**:** 483–486.
4. Frampton MW. Systemic and cardiovascular effects of airway injury and inflammation: Ultrafine particle exposure in humans. *Environ Health Perspect* 2001; **109**(Suppl 4)**:** 529–532.
5. Borm PJ, Kreyling W. Toxicological hazards of inhaled nanoparticles: Potential implications for drug delivery. *J Nanosci Nanotechnol* 2004; **4:** 521–531.
6. Seaton A, MacNee W, Donaldson K, Godden D. Particulate air pollution and acute health effects. *Lancet* 1995; **345:** 176–178.
7. Liao D, Creason J, Shy C, Williams R, Watts R, Zweidinger R. Daily variation of particulate air pollution and poor cardiac autonomic control in the elderly. *Environ Health Perspect* 1999; **107:** 521–525.
8. Nemmar A, Hoet PH, Vanquickenborne B, Dinsdale D, Thomeer M, Hoylaerts MF, et al. Passage of inhaled particles into the blood circulation in humans. *Circulation* 2002; **105:** 411–414.
9. Nemmar A, Hoylaerts MF, Hoet PH, Nemery B. Possible mechanisms of the cardiovascular effects of inhaled particles: Systemic translocation and prothrombotic effects. *Toxicol Lett* 2004; **149:** 243–253.
10. Seaton A, Donaldson K. Nanoscience, nanotoxicology, and the need to think small. *Lancet* 2005; **365:** 923–924.
11. Yamawaki H, Pan S, Lee RT, Berk BC. Fluid shear stress inhibits vascular inflammation by decreasing thioredoxin-interacting protein in endothelial cells. *J Clin Invest* 2005; **115:** 733–738.
12. Yamawaki H, Lehoux S, Berk BC. Chronic physiological shear stress inhibits tumor necrosis factor-induced proinflammatory responses in rabbit aorta perfused ex vivo. *Circulation* 2003; **108:** 1619–1625.
13. Martinet W, De Bie M, Schrijvers DM, De Meyer GR, Herman AG, Kockx MM. 7-ketocholesterol induces protein ubiquitination, myelin figure formation, and light chain 3 processing in vascular smooth muscle cells. *Arterioscler Thromb Vasc Biol* 2004; **24:** 2296–2301.
14. Bravo R, Macdonald-Bravo H. Existence of two populations of cyclin/proliferating cell nuclear antigen during the cell cycle: Association with DNA replication sites. *J Cell Biol* 1987; **105:** 1549–1554.
15. Charo IF, Taubman MB. Chemokines in the pathogenesis of vascular disease. *Circ Res* 2004; **95:** 858–866.
16. Kusano KF, Nakamura K, Kusano H, Nishii N, Banba K, Ikeda T, et al. Significance of the level of monocyte chemoattractant protein-1 in human atherosclerosis. *Circ J* 2004; **68:** 671–676.
17. Blankenberg S, Barbaux S, Tiret L. Adhesion molecules and atherosclerosis. *Atherosclerosis* 2003; **170:** 191–203.
18. Ross R. The pathogenesis of atherosclerosis: A perspective for the 1990s. *Nature* 1993; **362:** 801–809.
19. Ross R. Atherosclerosis: An inflammatory disease. *N Engl J Med* 1999; **340:** 115–126.
20. Moncada S, Palmer RM, Higgs EA. Nitric oxide: Physiology, pathophysiology, and pharmacology. *Pharmacol Rev* 1991; **43:** 109–142.
21. Lam CW, James JT, McCluskey R, Hunter RL. Pulmonary toxicity of single-wall carbon nanotubes in mice 7 and 90 days after intratracheal instillation. *Toxicol Sci* 2004; **77:** 126–134.
22. Peters K, Unger RE, Kirkpatrick CJ, Gatti AM, Monari E. Effects of nano-scaled particles on endothelial cell function in vitro: Studies on viability, proliferation and inflammation. *J Mater Sci Mater Med* 2004; **15:** 321–325.
23. Kondo T, Kobayashi K, Murohara T. Nitric oxide signaling during myocardial angiogenesis. *Mol Cell Biochem* 2004; **264:** 25–34.
24. Kwak BR, Mulhaupt F, Veillard N, Gros DB, Mach F. Altered pattern of vascular connexin expression in atherosclerotic plaques. *Arterioscler Thromb Vasc Biol* 2002; **22:** 225–230.
25. Yeh HI, Lu CS, Wu YJ, Chen CC, Hong RC, Ko YS, et al. Reduced expression of endothelial connexin37 and connexin40 in hyperlipidemic mice: Recovery of connexin37 after 7-day simvastatin treatment. *Arterioscler Thromb Vasc Biol* 2003; **23:** 1391–1397.
26. Suwannaprapha P, Chaisri U, Riyong D, Maneerat Y. Improvement of function and morphology of tumor necrosis factor-alpha treated endothelial cells with 17-beta estradiol: A preliminary study for a feasible simple model for atherosclerosis. *Circ J* 2005; **69:** 730–738.
27. Bannerman DD, Goldblum SE. Mechanisms of bacterial lipopolysaccharide-induced endothelial apoptosis. *Am J Physiol Lung Cell Mol Physiol* 2003; **284:** L899–L914.
28. van Rijen HV, van Kempen MJ, Postma S, Jongsma HJ. Tumour necrosis factor alpha alters the expression of connexin43, connexin40, and connexin37 in human umbilical vein endothelial cells. *Cytokine* 1998; **10:** 258–264.
29. Simon AM, McWhorter AR, Chen H, Jackson CL, Ouellette Y. Decreased intercellular communication and connexin expression in mouse aortic endothelium during lipopolysaccharide-induced inflammation. *J Vasc Res* 2004; **41:** 323–333.
30. Boerma M, Forsberg L, Van Zeijl L, Morgenstern R, De Faire U, Lemne C, et al. A genetic polymorphism in connexin 37 as a prognostic marker for atherosclerotic plaque development. *J Intern Med* 1999; **246:** 211–218.
31. Egashira K. Clinical importance of endothelial function in arterio-

sclerosis and ischemic heart disease. *Circ J* 2002; **66:** 529–533.
32. Vanhoutte PM. Endothelial control of vasomotor function: From health to coronary disease. *Circ J* 2003; **67:** 572–575.
33. Tsao PS, Buitrago R, Chan JR, Cooke JP. Fluid flow inhibits endothelial adhesiveness: Nitric oxide and transcriptional regulation of VCA, USAM-1. *Circulation* 1996; **94:** 1682–1689.
34. Garg UC, Hassid A. Nitric oxide-generating vasodilators and 8-bromo-cyclic guanosine monophosphate inhibit mitogenesis and proliferation of cultured rat vascular smooth muscle cells. *J Clin Invest* 1989; **83:** 1774–1777.
35. Wilkinson IB, Franklin SS, Cockcroft JR. Nitric oxide and the regulation of large artery stiffness: From physiology to pharmacology. *Hypertension* 2004; **44:** 112–116.
36. Boutouyrie P, Tropeano AI, Asmar R, Gautier I, Benetos A, Lacolley P, et al. Aortic stiffness is an independent predictor of primary coronary events in hypertensive patients: A longitudinal study. *Hypertension* 2002; **39:** 10–15.
37. Cruickshank K, Riste L, Anderson SG, Wright JS, Dunn G, Gosling RG. Aortic pulse-wave velocity and its relationship to mortality in diabetes and glucose intolerance: An integrated index of vascular function? *Circulation* 2002; **106:** 2085–2090.
38. Bai Y, Suzuki AK, Sagai M. The cytotoxic effects of diesel exhaust particles on human pulmonary artery endothelial cells in vitro: Role of active oxygen species. *Free Radic Biol Med* 2001; **30:** 555–562.
39. US Environment Protection Authority. Air quality criteria for particulate matter. 1996. EPA report No. EPA-600/P-95/001cF.
40. Venners SA, Wang B, Xu Z, Schlatter Y, Wang L, Xu X. Particulate matter, sulfur dioxide, and daily mortality in Chongqing, China. *Environ Health Perspect* 2003; **111:** 562–567.